Synthesis of a New Chloro Antimony Complex with Pyridinium Derivative: Crystal Structure, Hirshfeld Surface Analysis, Vibrational, and Optical Properties

Nour Elleuch[1] · Donia Fredj[1] · Nassira Chniba-Boudjada[2] · Mohamed Boujelbene[1]

Abstract

The new organic–inorganic hybrid material $(C_6H_7N_2S)_2[SbCl_4]Cl$ was synthesized by slow evaporation method and characterized by single-crystal X-ray diffraction, infrared absorption, Hirshfeld surface analysis, optical absorption and photoluminescence measurements. The Centro symmetric compound crystallizes in the triclinic system of space group $P\bar{1}$ with two formula units cell (Z = 2). The crystal structure is composed of a discrete $[SbCl_4]^-$ anion and two isolated chloride Cl^- anions which carried the same negative charge to balance the total charge of this compound surrounded by the 4 pyridiniumethioamide cations. Organic and inorganic parts which are linked by means of hydrogen bonding contacts N–H···Cl with N···Cl length are varied in the range of 3.221–3.456 Å to form a Zero-dimensional network. The infrared study performed at room temperature charge in the 4000–400 cm^{-1} frequency regions confirms the existence of the organic cation $[C_6H_7N_2S]^+$ and that of the $[SbCl_4]^-$ anion. The Photoluminescence spectrum exhibits a broad and strong band of luminescence located at 1.95 eV (635 nm), which can be even observed with the naked eye at room temperature and is due to exaction emission. The various intermolecular interactions of the two independent cations and six chloride atoms were examined via Hirshfeld surface analysis.

Keywords Antimony material · X-ray diffraction · Hirshfeld surfaces · Vibrational spectroscopy · Luminescence

1 Introduction

The group of halogenoantimonates (III) and halogenobismuthates (III) organic–inorganic hybrids are interesting systems because of the opportunity to associate the organic and the inorganic materials properties.

In fact, the coordination compounds of the main group metals which are characterized by their ns^2 electronic lone pair at the metal, present a large variety of different structures. Among these complexes, the materials based on antimony (III) are good examples of this behavior. Nowadays, these compounds have received special attention for their various physical and chemical properties such as magnetic or ferroelectric transitions, conductivity (super conductivity), electroluminescence and photo-luminescence [1, 2]. In particular case of aromatic antimonate (III) chlorides, $[SbCl_4]^-$ anions are obtained [3, 4]. In these compounds, the metal shows a tendency towards distorted or regular tetrahedral coordination with some rather long Sb–Cl bonds. This allows us to compare the relative importance of the stereo chemical activity of the lone electron pair on the Sb(III). Typically, chloro antimonates (III) expose a wide range of interactions and offer a unique possibility to compare the relative importance of the stereo chemical activity of the lone electron pair on the Sb(III) atom and N–H···Cl hydrogen bonds [5]. These anionic species have been observed to form a variety of dimensionality. Indeed, the antimony halide often built up by distorted $[SbCl_6]^{3-}$ octahedra or $[SbCl_4]^-$ tetrahedron, which can be isolated or connected with each other by corners, edges, or faces, thus forming

✉ Mohamed Boujelbene
m_boujelbene2010@yahoo.fr

[1] Laboratoire Physico-Chimie de l'Etat Solide, LR11ES51, Faculté des Sciences de Sfax, Université de Sfax, Route de Soukra Km 3.5, BP 802, 3071 Sfax, Tunisia

[2] Laboratoire de Cristallographie, CNRS, 25 Avenue des Martyrs, BP 166, 380 Grenoble, France

naturally isolated molecules (0D) [6, 7], infinite chains (1D) [8] or two dimensional (2D) networks. More than 30 various anionic structures have been isolated so far [9, 10]. In these materials, the crystal packing is defined by the interaction between the two organic and inorganic entities, which can be hydrogen bonds, van der Waals, or electrostatic interactions. However, based on recent research works on organic–inorganic metal halides compounds taken as a support to study the effects of the size and the coordination mode of the cation, we have successfully synthesized a new Zero-dimensional organic–inorganic hybrid compound of the formula $(C_5H_7N_2S)_2[SbCl_4]Cl$. This research work reports the chemical synthesis, structure characterization by X-ray diffraction, infrared spectroscopy (IR), and optical (photoluminescence and absorption) properties of the 4 pyridiniumethioamide chloride tetrachloro antimonates (III).

2 Experimental

2.1 Synthesis

Under ambient conditions, the title compound $(C_6H_7N_2)_2[SbCl_4]Cl$ was synthesized by dissolving in about 10 ml of distillated water each one of 4 pyridinethioamide $C_6H_6N_2S$ (0.27 mg, 97%) and Antimony trichloride $SbCl_3$ (0.228 mg, 99.5%) which were purchased from Sigma–Aldrich and used without further purification. Then, these latter were mixed in the 2:1 stoichiometric ratio in a concentrated HCl (37%, 3 ml) as shown in the following reaction:

$$2(C_6H_6N_2S) + SbCl_3 + 2 HCl \xrightarrow{H_2O} (C_6H_7N_2S)_2[SbCl_4] Cl$$

The resulting aqueous solution was then kept to evaporate at room temperature for about 4 weeks, leading to the growth of yellow crystals of $(C_6H_7N_2S)_2[SbCl_4] Cl$.

2.2 Hirshfeld Surface Calculations

Hirshfeld surfaces analyses [11] and their associated two-dimensional fingerprint plots as a powerful tool leads not only to study the solid-state behavior of molecules, but also to qualify the different types of inter-molecular inter-actions in the title compound. Molecular Hirshfeld surfaces, which were generated by the Crystal Explorer program [12, 13], were constructed from CIF file in order to analyze crystal structures.

Molecular Hirshfeld surfaces are built based on the distribution of electrons calculated as the sum of spherical atom electron densities [14, 15]. Moreover, the d_{norm} normalized contact distance property between molecules in 3D space based on both d_i and d_e (The distance from Hirshfeld surface to the nearest nucleus inside and outside, respectively) and the van der Waals radii (r_i^{dvW} and r_e^{dvW}) of the atoms given by the following equation: [16, 17].

$$d_{norm} = \frac{d_i - r_i^{vdw}}{r_i^{vdw}} + \frac{d_e - r_e^{vdw}}{r_e^{vdw}}$$

Therefore, the values of d_{norm} can be negative or positive when intermolecular contacts were shorter or longer than "r^{vdw}", respectively.

The 3D d_{norm} surfaces were visualized using a red–white–blue color scheme as follows; the first one indicates a negative d_{norm} value; and a shorter intermolecular contact than $\sum r^{vdw}$, the second represents the distance close to van de Waals contacts with zero d_{norm} values, and the last one shows positive d_{norm} values and a longer intermolecular contact than $\sum r^{vdw}$. The combination of d_e and d_i in the form of a 2D fingerprint plot [18] ensures the summary of intermolecular contacts in the crystal and are in complement to the Hirshfeld surfaces [19]. Two additional colored properties (shape index and curvedness) based on the local curvature of the surface can also be specified [20]. The present research works adopt the Hirshfeld surfaces analysis which are mapped with d_{norm}, shape-index, curvedness and 2D fingerprint plots (full and resolved) and performed by the Crystal-Explorer program [21].

2.3 Infrared Measurements

To gain more information within the crystal structure, we have undertaken a vibrational study using the Fourier transform infrared (FT-IR) absorption at room temperature, which was performed, in a Perkin–Elmer FT-IR Paragon 1000 PC spectrometer over the 4000–400 cm^{-1} range, in a KBr pellet.

2.4 Absorption and Photoluminescence Measurements

The photoluminescence spectrum of $(C_6H_7N_2S)_2[SbCl_4]Cl$ was reported at room temperature in which we utilized a PerkinElmer LS 55 spectrometer within a 350 nm radiation.

The optical absorption spectrum was resolute from transmission measurements performed using Cary 5000 UV–Vis–NIR spectrophotometer.

2.5 X-ray Crystallography

A new single crystal was mounted at 293 K on a Bruker ApexII Kappa CCD diffractometer using AgKa radiation ($\lambda = 0.5608$ Å). A number of 28,517 reflections were measured, out of which 4650 were independent and 4211 had

Table 1 Crystal data and experimental parameters used for the intensity data collection strategy and final results of the structure determination
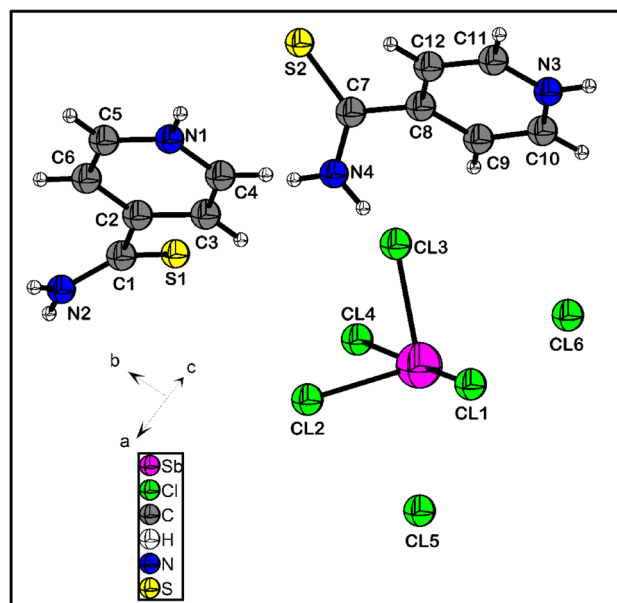
Chemical formula	$(C_5N_2H_7S)_2[SbCl_4]Cl$
Formula weight (g mol^{-1})	*874.38*
Crystal system, space group	*Triclinic,* $P\bar{1}$
Temperature	293 K
a (Å)	9.502 (5)
b (Å)	10.461 (5)
c (Å)	12.262 (5)
α (°)	115.250 (5)
β (°)	109.376 (5)
γ (°)	90.251 (5)
Cell volume (Å^3)	1024.6 (8)
Z	2
$F(000)$	832
Density	2.834
μ (mm^{-1})	2.16
Radiation type, λ (Å)	Ag $K\alpha$, 0.56087
R_{int}	0.055
Θ range (°)	2.7–21.4
Indexes range	$-12 \leq h \leq 12$
	$-13 \leq k \leq 13$
	$-15 \leq l \leq 15$
Measured reflections	28,517
Independent reflections	4650
Reflection with I > 2 σ(I)	4211
R[F2 > 2σ(F2)]	0.054
wR(F^2)	0.175
Goof S(F^2)	1.04
$\Delta\rho_{max}/\Delta\rho_{min}$ (e Å^{-3})	2.73/−3.15
Summary of data CCDC	1,888,302

Table 2 Hydrogen-bonds geometry (Å)

D–H	d(D–H)	d(H⋯A)	⟨DHA⟩	d(D⋯A)	A
N2–H2A	0.860	2.542	136.51	3.221	Cl1
N4–H4A	0.860	2.548	137.04	3.231	C14
N3–H3	0.860	2.958	114.38	3.405	C14
N3–H3	0.860	2.561	155.08	3.360	C15
N1–H1	0.860	2.947	115.51	3.407	C11
N1–H1	0.860	2.579	154.50	3.376	C16

Fig. 1 Asymmetric unit of the $(C_6H_7N_2S)_2[SbCl_4]Cl$ crystal

intensity I > 2σ(I). The crystal structure was solved by direct methods using the program SHELXS-2013 [22]. However, the antimony atoms were determined by the method of Patterson with SHELXS-2013 program [22], while the other atoms such as the organic moieties were found from successive Fourier calculations using SHELXL-2013 [23]. The hydrogen atoms of the CH, NH and NH$_2$ groups were fixed geometrically by the appropriate instructions of the program (AFIX 43, AFIX 43 and AFIX 93, respectively) [23]. After performing several refinement tests, we found that the final discrepancy factors R1 = 0.055 and WR2 = 0.175. The drawings were made with Diamond [24].

The crystallographic data for $(C_6H_7N_2S)_2[SbCl_4]Cl$ are summarized in Table 1. The hydrogen bonding parameters are represented in Table 2. The interatomic distances and bonds angles are listed in Table S1. A summary of atomic coordinates with Ueq is given in Table S2.

3 Results and Discussion

3.1 Crystallographic Study

The results of single-crystal X-ray diffraction analysis at room temperature reveal that the title compound crystallizes in the centrosymmetric triclinic $P\bar{1}$ space group. The cell dimensions are: a = 9.5018 (5) Å, b = 10.4618 (5) Å, c = 12.2616 (5) Å, α = 115.2500 (5)°, β = 109.3762 (5)°, γ = 90.2513 (5)° and V = 1024.6 (8) Å^3.

The asymmetric unit of $(C_5H_7N_2)_2[SbCl_4]Cl$ is made up of the part of anions which is composed of a tetrachloride antimonite and two isolated chloride Cl$^-$ anions, and the part of cations formed by two independent 4 pyridiniumethioamide organic cations (Fig. 1). Furthermore, these cations are interposed between the inorganic sheets forming zigzag chains (Fig. 4) which are linked via hydrogen bonds N–H⋯Cl with N⋯Cl length in the range of 3.221–3.456 Å (Table 2).
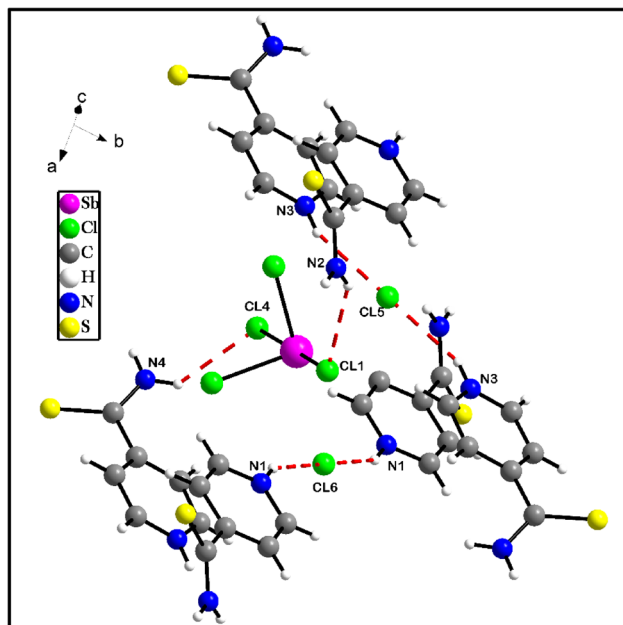
Fig. 2 The environment of the inorganic entities

In this atomic arrangement, the central antimony atom is surrounded by four chlorine atoms forming a regular $[SbCl_4]^-$ tetrahedral that are located at x = ¼ and x = ¾, They are also isolated from each other to form a Zero-dimensional network. Moreover, the geometry of the $SbCl_4$ tetrahedral chlorine coordination is characterized by a range of Sb–Cl bond length from 2.418(16) to 2.605(2) Å (Table S1) to
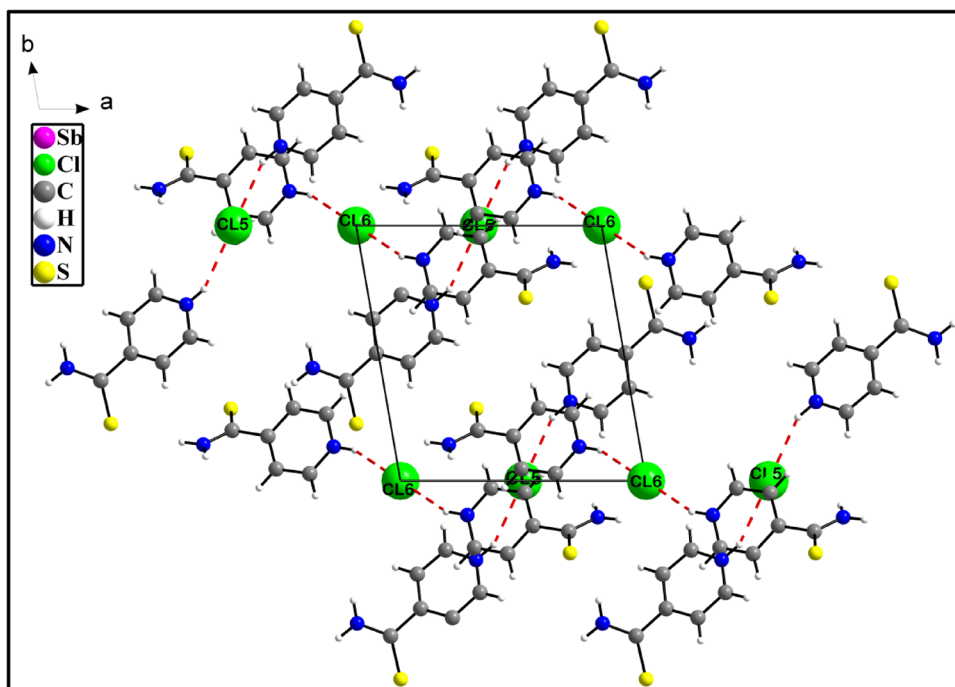
build a regular tetrahedron according to the result of distortion index [25] (Table S3):

$$ID(Sb-Cl) = 1/4 \sum_1^4 \left(\frac{SbCli - SbClm}{SbClm} \right) = 0$$

Table S1 generates the four Sb–Cl bonds ranging from 2.418 to 2.605 Å. The two longest ones (2.605 and 2.602 Å) correspond to (Cl(1)) and Cl(4), respectively. They are linked via the hydrogen bonds with the nitrogen atom (N(2)) and N(4) of 4 pyridiniumethioamide cation forming the shortest hydrogen bond N(2)–H···Cl(1) = 3.221 Å and N(4)–H···Cl(4) = 3.231 Å in this structure Table 2.

Figure 2 shows that anion part is surrounded by five cations where the $SbCl_4$ anion interconnected with one cation via hydrogen bond N(2)–H···Cl(1) whereas each chlorine of Cl6 and Cl5 is surrounded by two 4 pyridiniumethioamide via hydrogen bonds which are N(3)–H···Cl5 and N(1)–H···Cl6.

A projection of the structure on the (001) plane (Fig. 3) indicates that the inorganic clusters and $[C_6H_7N_2S]^+$ cations form alternating layers parallel to (a, b) plans, which are located at approximately x = ¼ and x = ¾ (Fig. 5).

It is evident that the intermolecular hydrogen bonding contacts N–H···Cl and the van der Waals contacts can give rise to a Zero-dimensional construction and add to stabilities.

Additionally, the free chloride anions Cl6 and Cl5 occupy the corners at x = 0 and the middle of the edge x = 1/2, respectively. Figures 3 and 4 show that the first one provides a linkage between two successive and similar chains

Fig. 3 The atomic arrangement of $(C_6H_7N_2S)_2[SbCl_4]Cl$ in projection along the c-axis

of 4 pyridiniumethioamide but the second one insures the connection between two cations into the chains.

Moreover, the molecular packing is dominated by hydrogen bonds interactions of the aforementioned type, which are formed by an intertial Cl atom (Cl6) and (Cl5) with 4 pyridiniumethioamide cations N(1)···Cl(6) 3.376 Å and N(3)···Cl(5) 3.360 Å.

The charge of the anionic sub lattice ($[SbCl_4]^- Cl_2^-$) is balanced by the presence of two independent cations each of which is mono-protonated $[C_6H_7N_2S]^+$. Indeed, the two chlorine anions share the same negative charge (Fig. 5, Table S2).

On the other hand, the organic cations are intercalating in the interlayer spacing and neutralize the negative charge of the inorganic layers. Furthermore, the distance between two aromatic nucleus was 6.617 Å > 3.8 Å (Fig. 6), which confirms that the π–π interaction are absent in this compound [26].

3.2 Infrared Spectroscopy

To gain more information about the structure of the title compound $(C_6H_7N_2S)_2[SbCl_4]Cl$, we performed a vibrational study using infrared absorption as shown in Fig. S1.

According to some studies reported in the literature [2, 27–35] we can propose an attempt of assignment of the observed bands Table 3.

The IR spectrum shows, at high wave numbers, the N–H stretching modes, combination bands and harmonics, whereas at lower ones, it indicates the bending and external modes. However, numerous functional groups such as NH, C–H, C–C, C–N, C–C–N and C–N–C are present in 4 pyridiniumethioamide cation, which are manifested in different range with different intensity (Fig. S1). The absorption bands observed at 3507 and 3329 cm^{-1} are attributed to the stretching asymmetric and symmetric υ(NH$_2$), respectively [28, 34]. However, scissoring asymmetric and symmetric vibration δ(NH$_2$) have been identified as broad and weak bands at 1717 and 1684 cm^{-1}, respectively [28, 34]. The bands at 1278, 692 and 674 cm^{-1} correspond to twisting NH$_2$ [29] and the band at 614 cm^{-1} is due to wagging (NH$_2$) [30]. Concerning the asymmetric stretching vibrations of the N–H bond, they appear at 3507, 1700 and 1684 cm^{-1} whereas the absorptions bands situated at 3329 and 1635 cm^{-1} correspond to the symmetric stretching vibration of the N–H bond (Fig. S1). Moreover, the broad band observed in the 2991–2685 cm^{-1} spectral region, corresponds to the NH stretching vibrations interconnected by a system of hydrogen bonds in the crystal [28, 32, 34].

Generally, in the caption 4 pyridiniumethioamide, the stretching vibrations C–H are detected in the region 2787–3133 cm^{-1} [28–32]. These vibrations are observed in IR at 3133, 2991, 2869 and 2787 cm^{-1}, where the two bands
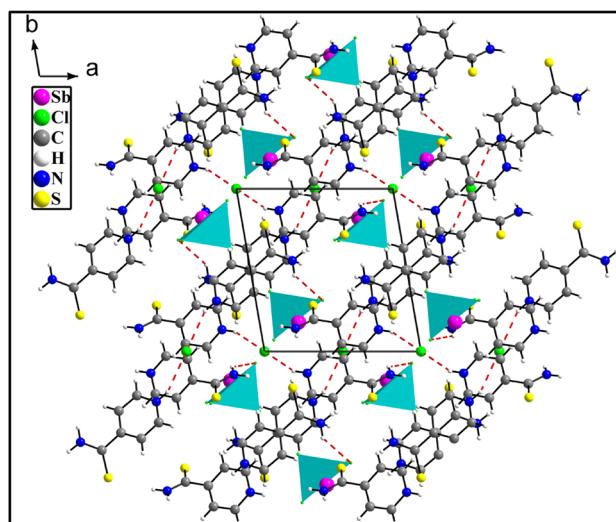
Fig. 4 Hydrogen bonds between Free chlorine and organic entities in the crystal structure of $(C_6H_7N_2S)_2[SbCl_4]Cl$ in projection along the c-axis. (H-bonds are represented by dashed lines)
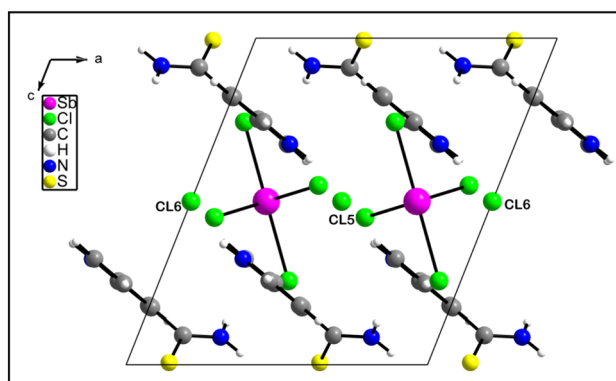

Fig. 5 The atomic arrangement of $(C_6H_7N_2S)_2[SbCl_4]Cl$ in projection along the b-axis

at 2904, 2869 cm^{-1} are attributed to the (C–H) asymmetric and symmetric stretching vibrations, respectively [33, 34].

Besides, the bands situated at 1204 and 1056 cm^{-1} were assigned to the in-plane bending (C–H) (Fig. S1). The vibrations at 1003 cm^{-1} are due to the scissoring mode of the N–H bands.

Additionally, the C=C stretching modes are superimposed in 1457, 1408 and 1388 cm^{-1}. Besides, the C–N asymmetric stretching modes are localized at 1129 cm^{-1} while C–N symmetric stretching mode was situated at 1232 cm^{-1}. The scissoring modes of the three bands C–N–H, C–C–C and C–C–N are observed at 1003, 464 and 446 cm^{-1}, respectively [31, 36]. The out-of-plane bending of (C–C–H) and C–H occurred at 845 and 812 cm^{-1}, respectively, as a medium peak [29]. Finally, the frequencies in the ranges of
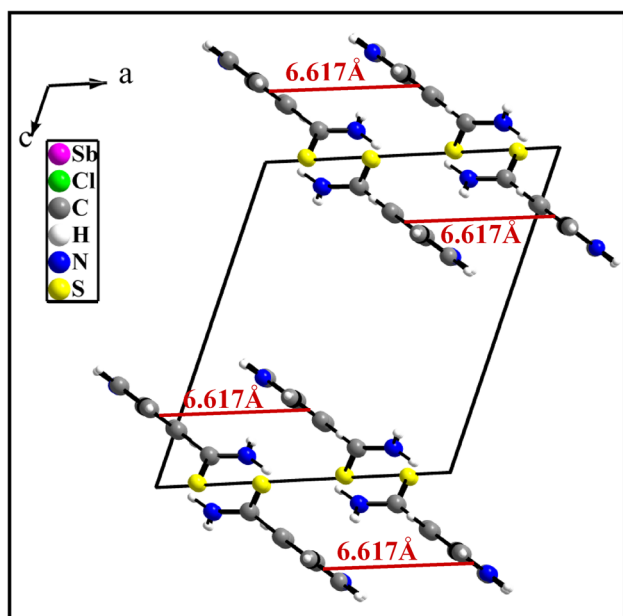
Fig. 6 Offset-face-to-face interactions motifs in the cation–cation chains in the plane (ab)

970–518 cm^{-1} and 764–416 cm^{-1} are attributed to the scissoring bending modes of C–C, C–N and C–NH$_2$ [31, 33, 34].

3.3 Optical Study

The optical properties of 4 pyridiniumethioamide chloride tetrachloroantimonates (III) were evaluated by the UV–Vis absorption and photoluminescence studies at room temperature. The obtained spectra are shown in Fig. 7, indicating that the $(C_6N_2H_7S)_2[SbCl_4]Cl$ exhibits two distinct absorption bands around 4.01 eV (310 nm) and 4.36 eV (285 nm) which are attributed to the metal charge transfer (LMCT) transition from the 3p orbital of Cl to 5p orbital of Sb(III) as described in previous outputs [35, 37–39]. On the other hand, the photoluminescence spectrum Fig. 7 shows a broad and strong emission band at 1.95 eV (635 nm), which can be even observed with the naked eye at room temperature and which is due to exciton emission [31, 36]. In the antimony (III) chloride based hybrids, the lowest exciton state arises from excitations between the valence band, which consists of a mixture of Sb(5s) and Cl(3p) states. Besides, the conduction band derives primarily from Sb(5p) states, and is confined zero-dimensionally network in the $[SbCl_4]^{-1}$ tetrahedron, which suggests that the material behaves as semiconductor and is consistent with the yellow color of the cristal.

Table 3 Experimental frequencies (cm^{-1}) of the $(C_5H_7N_2S)_2[SbCl_4]Cl$ compound

Observed FT-IR (cm^{-1})	Attributions
3329 m	$\upsilon_s(NH_2)$
3133 m	$\upsilon(C–H)$
2991 m	$\upsilon(N–H\cdots Cl)$
2904 m	$\upsilon_{as}(C–H)$
2869 vw	$\upsilon_s(C–H)$
2787 m	$\upsilon(C–H)$
2685 vw	$\upsilon(N–H\cdots Cl)$
1717 vw	$\delta_{as}(NH_2)$
1684 m	$\delta_{as}(NH_2)$
1635 m	$\delta(N–H)$
1580 bw	$\delta(N–H)$
1494 bw	$\beta(N–H)$
1457 bw	$\upsilon(C=C)$
1408 bw	$\upsilon(C=C)$
1388 m	$\upsilon(C=C)$
1339 m	$\upsilon_{as}(C–N)$
1278 s	$t(NH_2)$
1232 s	$\upsilon_s(C–N)$
1204 m	$\beta(C–H)$
1129 bw	$\upsilon(C–N)$
1087 bw	$\upsilon_{as}(C–C–N)$
1056 bw	$\beta(C–H)$
1025 bw	$\upsilon_s(C–C)$
1003 m	$\delta(C–N–H)$
970 m	$\delta(C–C)$
845 s	$\gamma(C–C–H)$
812 s	$\gamma(C–H)$
764 s	$\delta(C–N)$
734 m	$\gamma(C–H)$
729 vw	$\gamma(C–C–C)$
650 vw	$\delta(C–C)$
692 vw	$t(NH_2)$
674 m	$t(NH_2)$
614 bw	$\omega(NH_2)$
565 bw	$\delta(C–C=C)$
518 vw	$\delta(C–C)$
464 vw	$\delta(C–C–C)$
446 vw	$\delta(C–C–N)$
416 vw	$\omega(N–H) + \delta(C–NH_2)$

s Strong, *w* weak, *v* very, *b* broad, *m* medium, *υ* stretching, *β* in plane bending, *δ* scissoring, *ω* wagging, *t* twisting, *γ* out of plane bending

3.4 Molecular Hirshfeld Surfaces Analysis

The Hirshfeld surfaces has been conducted to explore the type of interactions (C–H···π, H···H, C···C etc.) as well as to study the various intermolecular interactions that play an important role in a molecular crystal. The molecular

Fig. 7 UV–Visible optical absorption (*a*) and Photoluminescence (*b*) spectrum of $(C_6H_7N_2S)_2[SbCl_4]Cl$
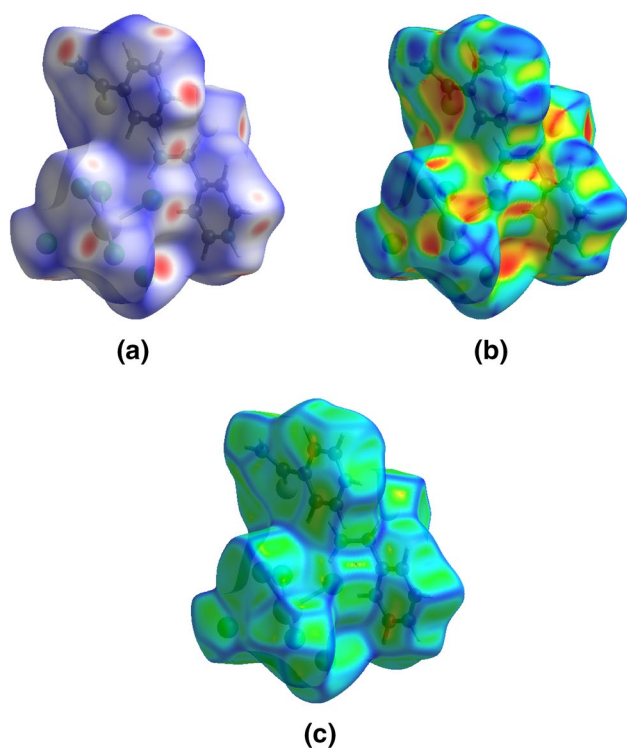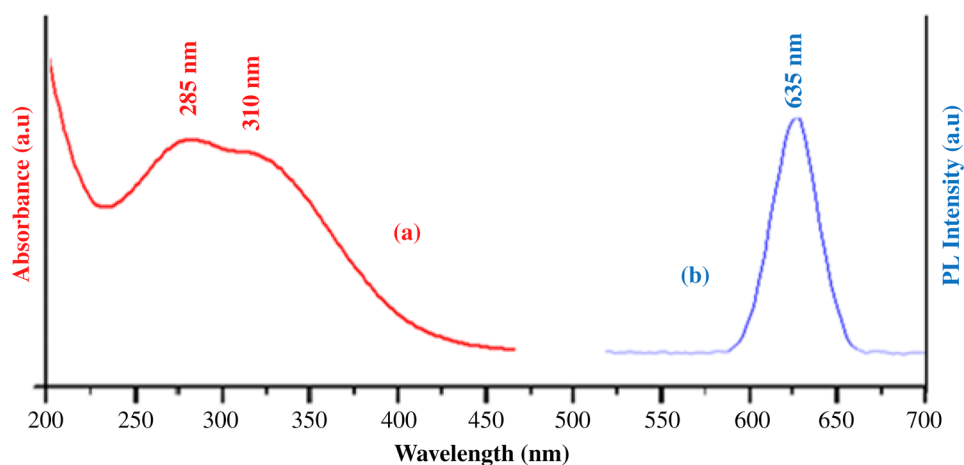
Fig. 8 Hirshfeld surfaces of 4 pyridinumethioamide dichloride tetrachloroantimonates(III): **a** 3D d_{norm} surface, **b** surface index, **c** curvedness

Hirshfeld surface; 3D d_{norm}, shape index and curvedness for $(C_6N_2H_7S)_2[SbCl_4]Cl$ are illustrated in (Fig. 8), showing surfaces that have been mapped over d_{norm} ranges from − 0.385 to 1.114 Å, shape index ranges from − 0.997 to 0.998 Å, and curvedness ranges from − 4.183 to 0.378 Å, respectively. The d_{norm} mapping indicates that strong hydrogen bond interactions, such as N–H···Cl hydrogen bonding between amino group and chloride appears as the main interaction

between the complexes, seen as a bright red area in the Hirshfeld surfaces (Fig. 8a).

The superseding H···Cl interactions are viewed in Hirshfeld surfaces by the bright red area in Fig. 8a which appear as distinct spike in the 2D fingerprint plots (Fig. 9). Visible complementary regions are visible in the fingerprint plots where one molecule acts as a donor ($d_e > d_i$) and the other as an acceptor ($d_e < d_i$).The 2D fingerprint plots of the title compound (Fig. 9) point out the strong intermolecular contacts which are Cl–H, N–H, C–H and S–H. In fact, the H···Cl/Cl···H interactions are predominant in the title compound with the major contributions 50.8% (Fig. 9). Moreover, the point in the (d_e, d_i) range of (1.58 Å, 0.95 Å) in the fingerprint plots are due to N–H···Cl interactions. The other visible spots were attributed to S···H/H···S contacts (16.5%), the proportion of H···H interactions present 9.2%, whereas, the relative contributions for C···H/H···C, C···C and N···H/H···N contacts are 5%, 2.6% and 2.1% respectively.

Figure 10 shows the percentages of contributions for all contacts in the title compound.

This constitutes evidence that Van-Der-Waals forces can enhance the stabilization of the packing. The shape index is highly sensitive to very subtle changes in surface shape. Indeed, the shape index (S) is 0D dimensionless surface property defined in terms of the two principal curvatures of the surface and can be used to distinguish complementary hollows(S = − 1.0; concave region; red colored) and bumps (S = + 1.0; convex region; blue colored) where two molecular Hirshfeld surfaces come into contact [18].Generally, the red and blue adjacent strangles on a shape index map provide π–π interaction information [15, 18, 40]. However, in this compound the π–π interactions were absent as presented in Fig. 8b. Thus, the Hirshfeld surface confirms the absence of the π–π stacking interactions in organic cations. The curvedness is a measure of the shape of the surface area of the molecule. The flat areas of the surface as revealed in Fig. 8c correspond to low values of curvedness, while sharp

Fig. 9 Fingerprint plot (de vs. di) of $(C_6H_7N_2S)_2[SbCl_4]Cl$ involving C⋯C interactions
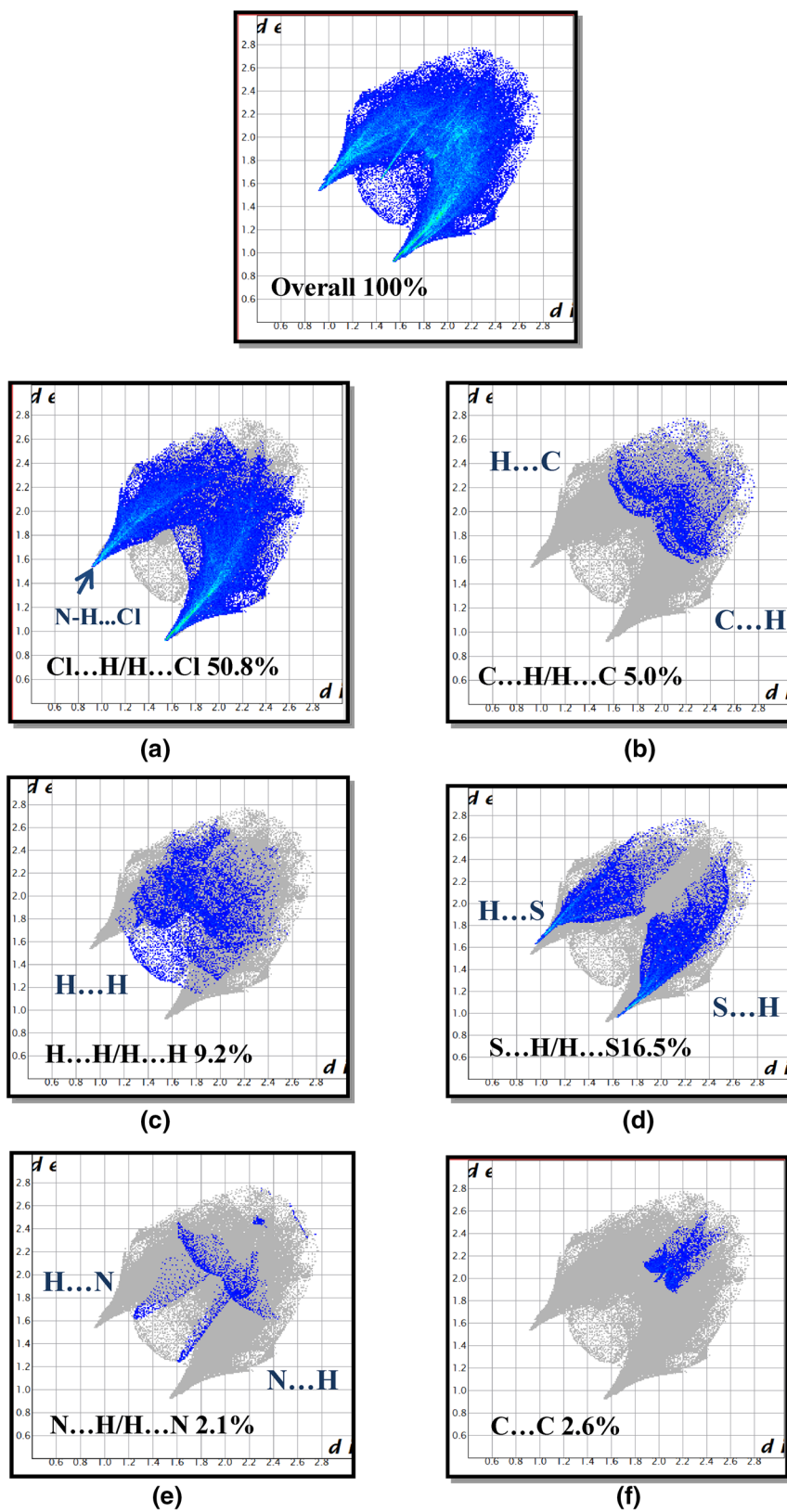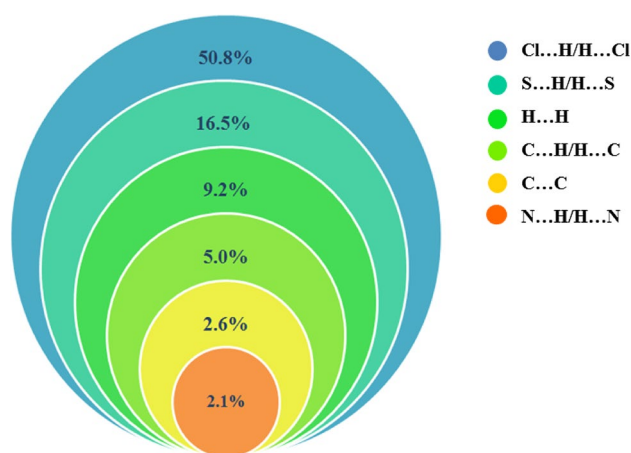
Fig. 10 Percentage contributions of the various intermolecular contacts contributing to the Hirshfeld surfaces of $(C_6H_7N_2S)_2[SbCl_4]Cl$

curvature areas correspond to high values of curvedness and usually tend to divide the surface into patches, indicating interactions between neighboring molecules. Moreover, the small range of area and light color on the surface indicate a weaker and longer contact other than hydrogen bonds. The large flat region which delineated by a blue outline refers to the π–π staking interactions. It is obvious that the curvedness of the complex reveals the absence of π–π stacking interactions in this complex Fig. 8c [41, 42].

4 Conclusion

The zero-dimensional hybrid compound $(C_6N_2H_7S)_2[SbCl_4]Cl$ structure consists of discrete $[SbCl_4]^-$ anion and two isolated chloride Cl anions. The atomic arrangement shows an alternations of organic and inorganic layers parallel to the [001] direction which are themselves linked via hydrogen bonds involving Cl$^-$ anions (N–H···Cl) forming a self-assembled zero-dimensional network. Fingerprint plots based on Hirshfeld surfaces analysis shows the various types of intermolecular interactions in this material.

In addition, the vibrational modes of this structure were studied by infrared spectroscopy, which were assigned by comparison with similar compounds.

5 Supplementary Materials

CCDC 1888302 include supplementary crystallographic data for this paper. This data can be obtained free of charge via http://www.ccdc.cam.ac.uk/conts/retrieving.html, or from the Cambridge Crystallographic Data Centre, 12 Union Rood, Cambridge CB2 1EZ, UK (Fax: (international): +44 1223/336 033; e-mail: deposit@ccdc.cam.ac.uk).

References

1. D.B. Mitzi, Prog. Inorg. Chem. **48**, 1 (1999)
2. H. Dammak, S. Triki, A. Mlayah, Y. Abid, H. Feki, J. Lumin. **166**, 180 (2015)
3. A. Lipka, D. Mootz, Z. Anorg, Allg. Chem. **440**, 231 (1978)
4. K. Kozawa, T. Uchicha, Acta Crystallogr. C **46**, 1006 (1990)
5. M. Bujak, J. Zaleski, J. Mol. Struct. **647**, 121 (2003)
6. J. Tarasiewicz, R. Jakubas, J. Baran, J. Vib. Spectrosc. **18**, 203 (1998)
7. A. Samet, H. Boughzala, H. Khemakhem, Y. Abid, J. Mol. Struct. **984**, 23 (2010)
8. B. Wenhua, N. Leblanc, N. Mercier, P. Auban-Senzier, C. Pasquier, Chem. Mater. **21**, 4099 (2009)
9. R. Jakubas, L. Sobczyk, Phase Transit. **20**, 163 (1990)
10. M. Hall, M. Nunn, M.J. Begley, D.B. Sowerby, J. Chem. Soc. Dalton Trans. **6**, 1231 (1986)
11. S.K. Wolff, D.J. Grimwood, J.J. Mckinnon, D. Jayatilaka, M.A. Spackman, *Crystal Explorer 2.0* (University of Western Australia, Perth, Australia, 2007)
12. S.K. Seth, D. Sarkar, A.D. Jana, T. Kar, J. Cryst. Growth Des. **11**, 4837 (2011)
13. M.A. Spackman, J.J. McKinnon, D. Jayatilaka, CrystEngComm **10**, 377 (2008)
14. M.A. Spackman, P.G. Byrom, Chem. Phys. Lett. **267**, 215 (1997)
15. M.A. Spackman, D. Jayatilaka, CrystEngComm **11**, 19 (2009)
16. A.L. Rohl, M. Moret, W. Kaminsky, K. Clabor, J.J. Mckinnon, B. Kahr, Cryst. Growth Des. **8**, 45 (2008)
17. A. Parkin, G. Barr, W. Dong, C.J. Gilmore, D. Jayatilaka, J.J. Mickinnon, M.A. Spackman, C.C. Wilson, CrystEngComm **9**, 648 (2007)
18. M.A. Spackman, J. McKinnon, CrystEngComm **4**, 378 (2002)
19. J.J. Koenderink, A.J. van Doorn, Image Vis. Comput. **10**, 557 (1992)
20. S.K. Wolff, D.J. Grimwood, J.J. Mckinnon, M.J. Turner, D. Jayatilaka, M.A. Spackman, *Crystal Explorer 2.2* (University of Western Australia, Crawley, 2010)
21. S.K. Seth, D. Sarkar, A.D. Jana, T. Kar, J. Cryst, Growth Des. **11**, 4837 (2011)
22. G.M. Sheldrick, *SHELXS-2013, Programs for Crystal Solution* (University of Gottingen, Germany, 2013)
23. G.M. Sheldrick, *SHELXL-2013, Programs for Crystal Structure Refinement* (University of Göttingen, Germany, 2013)
24. K. Brandenburg, Diamond Version 2.0 Impact GbR, Bonn, Germany (1998)
25. S. Shit, C. Marshner, S. Mitra, Acta. Chim. **63**, 129 (2016)
26. C. Hrizi, C. Chaker, S. Chaabouni, Ionics **17**, 545 (2011)
27. Y. Baklouti, N. Chaari, H. Feki, N. Chniba-Boudjada, F. Zouar, J. Spectrochim. Acta Part A **136**, 397 (2015)
28. D. Fredj, C. Ben Hassen, S. Elleuch, H. Feki, N. Chniba Boudjada, T. Mhiri, M. Boujelbene, J. Mater. Res. Bull. **85**, 23 (2017)
29. H. Dammak, H. Feki, H. Boughzala, Y. Abid, Spectrochim. Acta Part A **137**, 1235 (2015)

30. C. BenHassen, T. Dammak, N. Chniba-Boudjada, T. Mhiri, M. Boujelbene, J. Mol. Struct. **1127**, 43 (2017)
31. C. Hrizi, N. Chaari, Y. Abid, N. Chniba Boudjaba, S. Chaabouni, Polyhedron **46**, 41 (2012)
32. S. Chaouachi, S. Elleuch, B. Hamdi, R. Zouari, J. Mol. Struct. **1125**, 149 (2016)
33. H. Ferjani, H. Boughzala, A. Driss, J. Crystallogr. **8**, 2 (2013)
34. Z. Aloui, V. Ferretti, S. Abid, F. Lefebvre, M. Rzaigui, C. Ben Nasr, J. Mol. Struct. **1097**, 166 (2015)
35. A. Vogler, H. Nikol, Pure Appl. Chem. **64**, 1311 (1992)
36. H. Dammak, A. Yangui, S. Triki, Y. Abid, H. Feki, J. Lumin. **161**, 214 (2015)
37. H. Ferjani, H. Boughzala, J. Mater. **2013**, 8 (2014)
38. A. Samet, A. Ben Ahmed, A. Mlayah, H. Boughzala, E.K. Hlil, Y. Abid, J. Mol. Struct. **977**, 72 (2010)
39. A. Vogler, H. Nikol, Comments Inorg. Chem. **14**, 245 (1993)
40. R.S. Bitzer, C. Lorenzo, M. Horner, A.C. Marco Nascimento, C.A.L. Filgueiras, J. Mol. Struct. **1130**, 165 (2017)
41. Y.H. Luo, G.G. Wu, S.L. Mao, B.W. Sun, Inorg. Chim. Acta **397**, 1 (2013)
42. Y. Li, C.G. Zhang, L.Y. Cai, Z.-X. Wang, J. Coord. Chem. **66**, 3100 (2013)

Publisher's Note Springer Nature remains neutral with regard to jurisdictional claims in published maps and institutional affiliations.